

Comparison of automated crater catalogs for Mars from Benedix et al. (2020) and Lee and Hogan (2021)

C. Lee ¹

¹University of Toronto
¹60 St. George St., Toronto, Ontario, Canada

Key Points:

- The apparent performance of automatic crater detection algorithms is sensitive to the choice of metric used to gauge the performance.
- Feature Detection Algorithms trained to find spatial features should be used with appropriately projected images where possible.
- As neural networks extend crater detection beyond practical human limits, validating their results with independent networks is critical.

arXiv:2308.14650v1 [astro-ph.EP] 28 Aug 2023

Abstract

Crater mapping using neural networks and other automated methods has increased recently with automated Crater Detection Algorithms (CDAs) applied to planetary bodies throughout the solar system. A recent publication by Benedix et al. (2020) showed high performance at small scales compared to similar automated CDAs but with a net positive diameter bias in many crater candidates. I compare the publicly available catalogs from Benedix et al. (2020) and Lee and Hogan (2021) and show that the reported performance is sensitive to the metrics used to test the catalogs. I show how the more permissive comparison methods indicate a higher CDA performance by allowing worse candidate craters to match ground-truth craters. I show that the Benedix et al. (2020) catalog has a substantial performance loss with increasing latitude and identify an image projection issue that might cause this loss. Finally, I suggest future applications of neural networks in generating large scientific datasets be validated using secondary networks with independent data sources or training methods.

Plain Language Summary

I have compared two computer programs that use neural networks to identify craters on solar system bodies. The crater catalogs created by these programs have been previously compared against an existing human-made catalog to measure their performance, but each comparison used a different method making it challenging to understand the difference between the catalogs. In this paper, I use the comparison methods from these two independent papers, discuss where the catalogs agree and disagree, and suggest why they disagree. I emphasize the need for more accurate and consistent methods to validate automatic crater-mapping programs, especially when it is impractical for humans to check the craters found by automated methods.

1 Introduction

Crater mapping using neural networks and other automated methods has increased in recent years with automated Crater Detection Algorithms (CDAs) applied to planetary bodies throughout the solar system including Mercury and the Moon (e.g., Silburt et al., 2019) Mars and Pluto (e.g., Lee & Hogan, 2021; Lee, 2018b; Benedix et al., 2020) and large asteroids (e.g., Latorre et al., 2023). These methods approach or exceed the performance of human experts at identifying craters from imagery and topography data and have recently produced catalogs that are too large to be validated by humans in a reasonable time (Lagain, Benedix, et al., 2021). In this work, I compare the results from two automatically generated catalogs for Mars and two additional catalogs described below. I calculate the performance metrics against a shared ground-truth and show how the different test criteria originally developed for these catalogs (Lee, 2019; Benedix et al., 2020) leads to different apparent quality of each catalog.

In the next section, I describe the catalogs and discuss some of the stated limitations of the neural networks and catalogs provided. I then reproduce the comparison algorithms from Lee (2019) and Benedix et al. (2020) and use both methods to calculate the performance of each crater catalog in this comparison. I compare the performances of these catalogs as a function of crater location and size and discuss the differences in performance. I also identify a possible calculation error in Benedix et al. (2020) and suggest a correction. Finally, I give my conclusions on this comparison and suggest ways to mitigate errors and improve future catalogs.

2 Methods

2.1 Catalogs

In this work, I compare two publicly available crater catalogs generated by neural networks, **Benedix** from Benedix et al. (2020) and **DeepMars2** from Lee and Hogan (2021). I also compare a catalog generated as part of Lee and Hogan (2021) (**irH1K**) but not separately published, and a new catalog based on Benedix et al. (2020) (**B_Rescaled**) that I created as part of this work to correct a proposed error in the original catalog.

The **Benedix** catalog was generated by Benedix et al. (2020) from infrared images of the planet using the “You Only Look Once” (Redmon et al., 2016; Redmon & Farhadi, 2018) neural network, reporting 328,833 detected craters at diameters between 1km and 200km, covering the surface between ± 65 degrees latitude. Following (Benedix et al., 2020), the trained network was used to identify 90 million small craters (Lagain, Benedix, et al., 2021), and the same authors have sought to validate the Robbins and Hynes (2012) catalog using computer-aided tools (Lagain, Bouley, et al., 2021). The **Benedix** catalog was downloaded for this work from the supplementary material of Benedix et al. (2020).

The **DeepMars2** catalog was generated by Lee and Hogan (2021) using digital terrain models (DTMs) of the surface and co-registered infra-red imagery using a ResUNET network (Diakogiannis et al., 2019). Two separate networks were trained using the same Robbins and Hynes (2012) catalog as the ground-truth with randomly selected swatches from across the planet that were re-projected onto an orthographic projection. In addition to the combined catalog that used DTMs and IR detections, a high-resolution IR catalog was also developed in Lee and Hogan (2021) but truncated to 3.5km diameter and above to match the DTM limitations. In the following sections, we relax this constraint and include this infra-red imagery catalog truncated to a minimum of 1km in diameter (labeled as **irH1k**). The **DeepMars2** catalog was downloaded for this work from the associated BorealisData repository for the Lee and Hogan (2021) paper at Lee and Hogan (2020). The **irH1k** catalog was created as part of Lee and Hogan (2021) but is made available on the BorealisData repository associated with this work at Lee (2023b).

Finally, as part of this work, a possible error was identified in the **Benedix** catalog, and a correction was applied to create the **B_Rescaled** catalog. The correction involved rescaling the calculation of the pixel-to-geophysical size, resulting in smaller crater sizes at high latitudes in the new catalog. The **B_Rescaled** catalog is available from the BorealisData repository associated with this work at Lee (2023b).

Newer models have been developed since Benedix et al. (2020) and Lee and Hogan (2021), but typically examine a small area of Mars as validation (Yang & Cai, 2022; Giannakis et al., 2023) and provide no publicly accessible crater catalogs. There have also been improvements in surface imagery since Robbins and Hynes (2012) with improved geo-location of images (Robbins, 2017) and higher resolution visible imagery (<http://murray-lab.caltech.edu/CTX/>) from the Mars Reconnaissance Orbiter Context Camera (Malin et al., 2007).

In the rest of this paper, I refer to the algorithms and catalogs from Lee and Hogan (2021), Benedix et al. (2020), and Robbins and Hynes (2012). To avoid misattribution, I refer to the catalogs by their names above (**Benedix**, **DeepMars2**, **irH1K**, **B_Rescaled**, and **Robbins**) in the text and figures, and use the acronyms L19 (Lee, 2019) and B20 (Benedix et al., 2020) to refer to the comparison methodology developed by those authors.

2.2 Ground Truth Comparison methodology

Both Lee and Hogan (2021) and Benedix et al. (2020) compare their results against the **Robbins** catalog as a source of ‘ground-truth’. In each paper, the comparison re-

quired matching every crater from the CDA catalog with a crater in the **Robbins** catalog and required the definition of a matching algorithm. The L19 algorithm uses the following criteria to determine a positive crater match to the ground-truth:

$$\begin{aligned} F_D &= \frac{D_C - D_G}{\min(D_C, D_G)} \leq 0.25, \\ F_Y &= \kappa_Y \frac{Y_C - Y_G}{\min(D_C, D_G)} \leq 0.25, \\ F_X &= \kappa_X \frac{X_C - X_G}{\min(D_C, D_G)} \leq 0.25. \end{aligned} \quad (1)$$

Where D, X, Y are the diameter (km), longitude (degrees), and latitude (degrees) for the catalog crater (C) and ground-truth crater (G). $\kappa_Y = \frac{2\pi R_{\text{mars}}}{360}$ and $\kappa_X = \kappa_Y \cos Y_R$ convert from distance in degrees to distance in kilometers for a spherical planet.

A positive match is identified in L19 only when all three criteria (F_D, F_Y, F_X) are below 0.25. That is, when a candidate crater and ground-truth crater are both within 25% of the smaller crater’s diameter, and the centers of the two craters are within 25% of the smaller crater’s diameter.

Based on Benedix et al. (2020), the B20 method uses the following criteria to determine a positive crater match:

$$\begin{aligned} F_D &= \frac{D_C - D_G}{\min(D_C, D_G)} \leq 0.5, \\ F_Y &= \frac{Y_C - Y_G}{|Y_G|} \leq 0.02, \\ F_X &= \frac{X_C - X_G}{|X_G|} \leq 0.02. \end{aligned} \quad (2)$$

A positive match is identified in B20 if the diameters are within 50% and the crater centers are within 2% of their absolute location in longitude or latitude. Note that the B20 method doesn’t compare location relative to the diameter as L19 does, using the location in degrees in the denominator instead. B20 also allows matches when the craters do not overlap, while L19 requires an overlap by construction (the center of one crater must be within the circle representing the matching crater).

2.3 Comparison Metrics

I calculated the performance of the catalogs with respect to the ground-truth catalogs using the standard metric calculations (e.g., Lee, 2019; Goodfellow et al., 2016) that are also used in Lee and Hogan (2021) and Benedix et al. (2020).

Each candidate catalog is constructed from a number N_C total craters, compared to N_G ground-truth craters. Comparing these catalogs identifies a number N_T matching craters (‘true positive’) and N_F non-matching craters (‘false positive’). The performance metrics are all calculated using these crater counts. *Recall* is the fraction of craters in the ground-truth catalog that also exists in the candidate catalog: $R = N_T/N_G$. *Precision* is the fraction of craters in the candidate catalog that exists in the ground-truth catalog $R = N_T/N_C$. Since these metrics measure two distinct properties of the catalog, a blended metric (F_1 score) is also typically used, defined as the harmonic mean of *Precision* and *Recall*: $F_1 = 2PR/(P + R)$.

All three metrics are typically expressed as percentages. For example, Benedix et al. (2020) reported their catalog has a *Recall* of 77% and *Precision* of 75% (their table 1), Lee and Hogan (2021) reported their catalog has a *Recall* of 80% and *Precision* of 87% (their table 1). However, since these catalogs have different bounds on diameter and different spatial coverage, a direct comparison of these numbers is not practical.

For the CDA craters with a matching ground-truth crater (i.e., craters part of the N_T count above), I also calculated the percentage errors between matching pairs of craters based on equations 2 and 1 above. The percentage errors are then aggregated and plotted as histograms following figure 3 of Benedix et al. (2020). Since the L19 method cal-

culated errors relative to diameter, these errors cannot be directly compared with the B20 method, but the diameter errors used the same calculation and can be compared.

For each matching crater, I also calculated the Intersection-Over-Union (IOU) metric that measures the overlap (intersection) of two features relative to the total exposed surface area (union) (e.g., Fairweather et al., 2022; Benedix et al., 2020). The IOU calculation takes the pair of matching craters and calculates the ratio

$$IOU = \frac{\text{Total intersecting area of the crater pair}}{\text{Total exposed area of the crater pair}}$$

Perfectly overlapping craters have a maximum value of $IOU = 1$, while non-overlapping craters have a value of $IOU = 0$. Values between 0 and 1 include mismatched sizes and locations but require some overlap. For each of the matched crater pairs, I calculated the IOU metric assuming circular craters since all of the catalogs used in this comparison report crater parameters assuming circular features, even where the underlying craters are degraded or elliptical.

Finally, I calculated the *Recall* and *Precision* as a function of location and size to show the performance of each network across the planet and as a function of crater diameter. In principle, an unbiased network should perform equally well across the planet but will perform worse as the crater size approaches the native image scale and crater features become harder to detect.

Note that the main text of Benedix et al. (2020) also describes an ‘uncorrelated crater’ that is calculated in their table 1 as the number of ground-truth craters not found by the CDA (usually called a ‘false negative’), but it is described as indicating “where the algorithm found a crater that is not present in the [ground-truth].”. Similarly, their ‘false positive’ craters are described as being found by the ground-truth but not by the CDA (their section 3.3). These definitions are reversed compared to normal usage, and in their (Benedix et al., 2020) supplementary material S3 and their table 1 the calculations follow the standard definitions given above.

3 Results

Four catalogs are used in this section. The **DeepMars2** catalog from Lee and Hogan (2021), the **irH1k** infra-red channel catalog from Lee and Hogan (2021), the **Benedix** catalog from Benedix et al. (2020), and my attempted correction to the **Benedix** catalog in the **B_Rescaled** catalog. Table 1 summarizes the performance of each catalog measured against the **Robbins** ground-truth catalog.

The table shows the performance for both the B20 and L19 methodology for craters from 1.5km to 10km in diameter within 65 degrees from the equator (the limits used in Benedix et al. (2020)). The values for the **Benedix** catalog differ by 2-3% compared to Benedix et al. (2020), but these numbers are sensitive to the numerical algorithm used to match craters. For example, I could increase the *Recall* and *Precision* by 2% by allowing each ground-truth crater to match multiple candidate craters, but it’s not clear that Benedix et al. (2020) allowed this to occur.

The performance values for the **DeepMars2** are consistent with Lee and Hogan (2021), with a 1% difference in both *Recall* and *Precision* caused by not removing ~ 100 overlapping craters in the ground-truth catalog for this work.

The B20 and L19 crater matching methods produce very different results. The effect is most noticeable in the **Benedix** catalog, where performance drops by 35 percentage points using the stricter L19 method (a factor of two in CDA performance), but **irH1k** also drops by 10% when changing from the B20 method to the stricter L19 method. In contrast, the **DeepMars2** is largely unaffected because most non-overlapping craters were removed during post-processing (Lee & Hogan, 2021).

Method	Test	R	P	F1	TP	FP	FN	test count
B20	DeepMars2	20	95	33	32,995	1,672	130,416	34,667
	Benedix	72	70	71	117,485	50,875	45,926	168,360
	B_Rescaled	72	73	72	117,239	43,033	46,172	160,272
	irH1k	76	74	75	124,190	44,215	39,221	168,405
L19	DeepMars2	20	92	32	32,013	2,654	131,398	34,667
	Benedix	36	35	35	58,777	109,583	104,634	168,360
	B_Rescaled	47	48	47	76,410	83,862	87,001	160,272
	irH1k	65	63	64	105,717	62,688	57,694	168,405

Table 1. Table of metrics for each catalog with respect to the Robbins and Hynek (2012) catalog for craters within 65 degrees of the equator and between 1.5km and 10km in diameter. Recall, Precision, and F1 are rounded percentages, while all other numeric columns are integer values. A total of 163,411 ground-truth craters were in the comparison. R=Recall, P=Precision, F1=harmonic mean score, TP=true positive count,FP=false positive count, FN=false negative count (maybe listed as *uncorrelated craters* in Benedix et al. (2020)),

Figure 1 shows the size frequency distribution using the same bins as Benedix et al. (2020) (20 diameter bins per log-decade). The plot shows that most catalogs have similar distribution shapes, even with different precision and recall metrics. The Salamunićcar et al. (2012) catalog is truncated above 25km, and it shows discretization artifacts at lower diameters, as does **DeepMars1** from Lee (2019). The **irH1k** catalog only processed images up to 1.3 degrees across (a maximum crater size of about 40km).

Figure 2 shows the distribution of errors for craters matched between a candidate catalog and the **Robbins** catalog using the B20 method (equation 2). The shapes of these figures agree reasonably well with Benedix et al. (2020). The location error is relatively unbiased with a prominent central peak, and the diameter errors shown here match the reported positive bias(Benedix et al., 2020). The **DeepMars2** catalog has a lower total count but similar biases to the **irH1K** catalog. The diameter biases have different signs between the Benedix et al. (2020) and Lee and Hogan (2021) catalogs, possibly due to a difference in network training.

Figure 3 shows the calculation of errors using the L19 method (equation 1). Note that all errors are now calculated relative to the diameter of the smaller crater in a matched pair since the L19 method included that diameter as the denominator in each calculation. The shape of the diameter plot is essentially the core of the same subplot in figure 2. In contrast, the longitude and latitude figures are functionally different, showing the position error *relative* to the crater diameter rather than in *absolute* location as in figure 2.

Figure 4 shows the distribution of Intersection-over-Union (IOU) values for matching craters using both methods (L19 in solid lines, B20 in dashed lines) and for each catalog relative to **Robbins**. We did not calculate IOU metrics in training the L19 or L21 CDA because the algorithm matched crater rims with narrow widths. Benedix et al. (2020) reported that validation and training were based on IOU comparisons with the ground truth and required a high threshold for a positive detection. The plot shows $IOU > 0.3$ for all matches in the L19 method (solid lines) compared to the theoretical minimum of $IOU \approx 0.25$ given the constraints in equation 1. Since the B20 method counts some non-overlapping craters as matches, there is a population of matching craters with no intersection and a value $IOU = 0$, marked with a horizontal line for each catalog at the left edge of the plot.

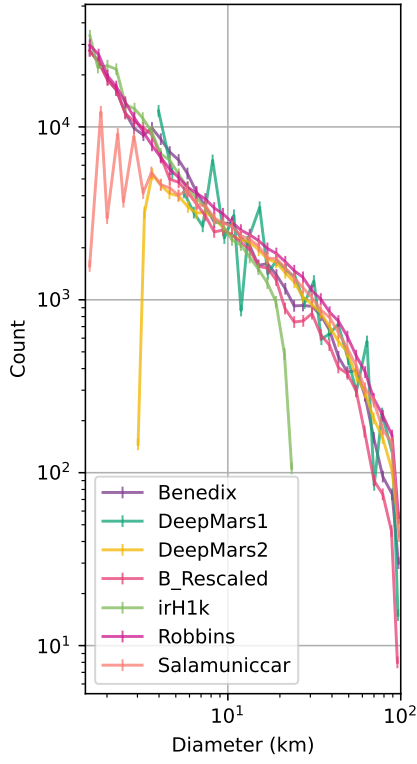


Figure 1. Size Frequency Distribution of all craters in each catalog. **Benedix** from Benedix et al. (2020), **DeepMars1** from Lee (2019) , **DeepMars2** from Lee and Hogan (2021), **irH1k** from the high resolution IR channel (Lee & Hogan, 2021), **Robbins** from Robbins and Hynek (2012), and **Salamuniccar** from Salamunićcar et al. (2012).

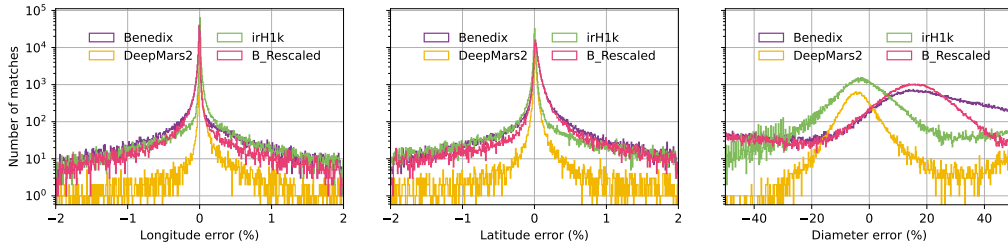


Figure 2. Distribution of errors in longitude (left), latitude (center), and crater Diameter (right) calculated according to the B20 method (equation 2) using 500 bins in each histogram. Calculations were made relative to the ground-truth catalog such that positive numbers imply a positive bias in the CDA catalog.

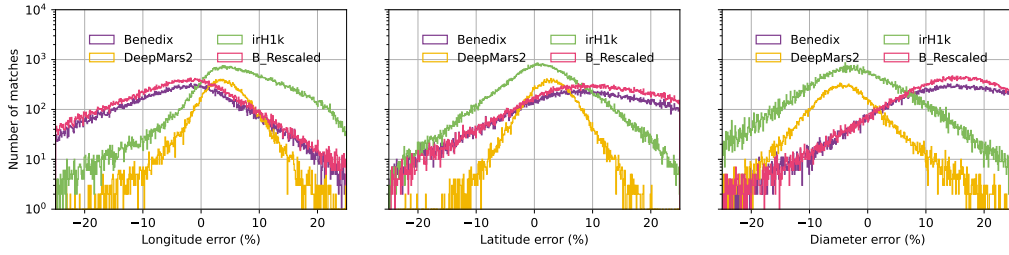


Figure 3. Distribution of errors in longitude (left), latitude (center), and crater Diameter (right) calculated according to the L19 method (equation 1). The horizontal extent of the longitude and latitude plot appear larger here but are expressed relative to the crater diameter rather than the absolute value of longitude or latitude used in figure 2. Calculations were made relative to the ground-truth catalog such that positive numbers imply a positive bias in the CDA catalog

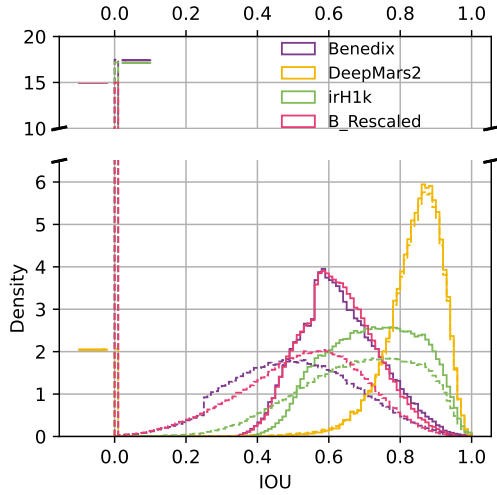


Figure 4. Intersection-over-Union values for the four crater catalogs. Solid lines show the IOUs of crater pairs matched using the L19 method. Dashed lines show the same catalogs matched using the B20 method, and horizontal lines at $IOU=0$ highlight the population of non-overlapping craters ($IOU = 0$) found using the B20 method. The histograms used 100 bins.

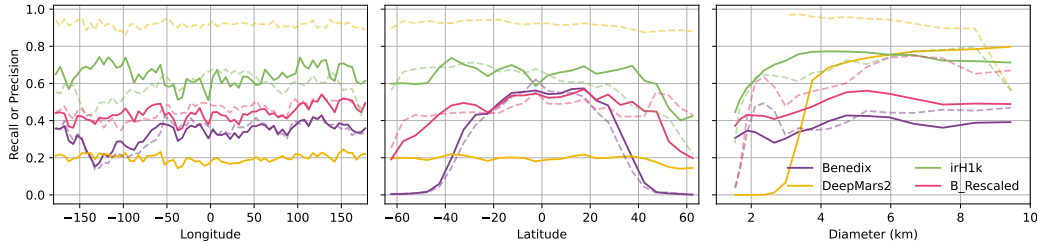


Figure 5. *Recall* (solid) and *Precision* (dashed) plotted as a function of longitude, latitude, and diameter for catalogs matched using the L19 method. Longitude and latitude are aggregated into 5-degree bins, and diameter is aggregated into 20 bins per log-decade.

Figure 5 shows the *Recall* and *Precision* metrics as a function of longitude, latitude, and diameter based on matched-craters using the L19 method. The **DeepMars2** catalog has the largest difference between *Recall* and *Precision* because it removes all craters below 3.5km in diameter and thus misses 100,000 small craters, lowering the *Recall* across all longitudes and latitudes. All four catalogs have consistent performance in longitude, fluctuating about 10% overall. In latitude, the **Benedix** catalog has a significant performance drop with increasing latitude in both hemispheres, while the **irH1k** has a small drop in performance with latitude with worse performance in the northern hemisphere. All four catalogs lose performance as the crater diameter approaches the pixel scale of the source imagery, as expected. For **DeepMars2**, this drop-off occurs at 3.5km. For the other (IR) catalogs, the drop-off occurs near 2km.

4 Discussion

To generate the comparisons, I needed to make several assumptions to reproduce the B20 method and crater-matching catalogs. Neither **Benedix** nor **DeepMars2** include the corresponding craters from **Robbins**. Instead, I built the crater-matching algorithms following the description in Benedix et al. (2020) (B20, equation 2 above) and Lee (2019) (L19, equation 1 above).

Using these two comparison methods, I identified craters that matched with a unique ground-truth crater and used these matches to generate the statistics presented here. The results in table 1 deviate by a few percent compared to Benedix et al. (2020), but these numbers can be adjusted by a percent or two in either direction by changing the interpretation of parameters in the matching algorithm. Still, the metrics are comparable within this work because they are all calculated with the same methodology and code. The SFD (figure 1) and the error distribution (figure 2) match well with the corresponding figures from Benedix et al. (2020), providing some confidence that the implementation of the B20 method matches the original. Similarly, the metrics and biases reported in Lee and Hogan (2021) agree with the values calculated here using the L19 method.

The B20 algorithm produced higher apparent performance because it included craters that don't overlap with their targets, accounting for 50% of **Benedix** matches, 3% of **DeepMars2**, and 16% of **irH1k**. The L19 algorithm required overlapping craters for a valid match and thus produced higher IOU distributions in figure 4 but lower overall performance. Craters that matched according to L19 also matched according to B20 except for the few craters along the equator or prime meridian where 2% of absolute longitude is smaller than 25% of the crater diameter.

The performance of each catalog is reasonably consistent with longitude and has the expected drop as the crater diameter approaches the image pixel scale. There is a drop in performance with latitude in the catalogs, but a much larger drop in performance with latitude in **Benedix** suggests a more fundamental error caused by neglecting to project images onto orthographic projections before processing.

The source of the error is not obvious from the available catalogs without access to the processing algorithms. However, of the 58,578 **Benedix** catalog craters matched by B20 but not by L19, only 13,383 would satisfy the diameter constraints of the L19 method. If the crater diameters in **Benedix** are affected by a projection error, or equivalently using the wrong pixel-to-kilometer scaling factor, they can be corrected in the existing dataset because the catalog includes pixel scale parameters and location information. Scaling the diameters by cosine latitude improves the catalog performance using the L19 method by allowing an additional 23,309 craters to match the ground-truth catalog.

This hypothesis is supported by the raw pixel size information provided in the **Benedix** catalog. Figure 6(top) shows the density map of craters as a function of the latitude and the ratio of the height ('dy') to width ('dx') of the rectangle encompassing the crater in pixel values. This ratio should be near 1 for orthographically projected images for circular craters at all latitudes, but has a cosine latitude dependence for Plate Carée (unprojected, or latitude-longitude) images. In unprojected images, circular craters appear stretched in longitude at higher latitudes, and the ratio dy/dx decreases for circular features, as shown in the figure. This issue suggests the image swatches were presented to the CDA as unprojected images where circular physical features appear elliptical in the images, and the CDA was trained to find horizontally stretched ellipses rather than circles.

The pixel level information can also be used to determine how the conversion to geophysical units (in this case, kilometers) was done by Benedix et al. (2020). Three image scales were used by Benedix et al. (2020), and these scales accurately map all of the report sizes in the 'x' dimension from the pixel size to the reported physical size of the crater in kilometers. However, in these images, 'x' corresponds to longitude and should have a different scaling with latitude, whereas the 'y' axis corresponds to the pixel scale in latitude and does not vary with location. Thus, the crater's pixel size in the 'y' axis should have been used instead of the size in 'x'. As a result, the **Benedix** catalog has an increasing positive bias in crater diameter as a function of latitude (figure 6(bottom)).

My proposed fix for this error is to apply the image pixel scaling to the 'dy' pixel values instead of 'dx', which produces the **B.Rescaled** catalog shown in each table and figure. This new catalog has improved global metrics, reduced errors, and increased IOU values relative to **Benedix**. The *Recall* and *Precision* metrics also remain higher with latitude and increase in all dimensions compared to the original catalog. However, this improvement does not definitively prove that the **Benedix** catalog has a projection issue, and other issues might cause the observed bias.

5 Conclusions

I have examined crater catalogs generated with neural networks (Lee & Hogan, 2021; Benedix et al., 2020) whose results suggested similar performance but were calculated using different methodologies. Using the comparison method from Lee (2019) I found that the Benedix et al. (2020) catalog has significantly lower *Precision* compared to Lee and Hogan (2021) generating 30 times more false crater detections, but did contain more craters in total and with a higher *Recall*. When compared to the infrared channel of Lee

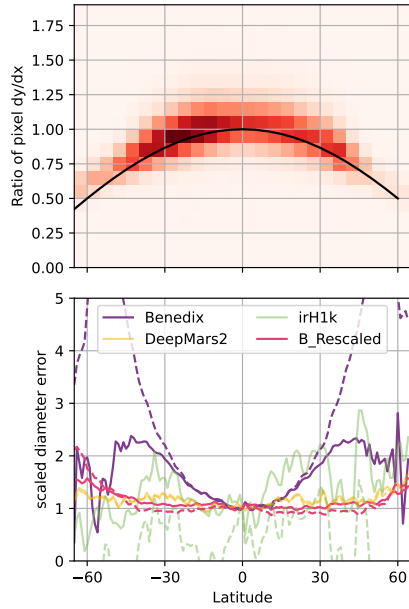


Figure 6. (top) Heat map of crater population as a function of latitude and the ratio of height-to-width (dy/dx) of the pixel-level rectangle in the **Benedix** catalog. Darker shades represent a higher density of craters, and the black line shows the cosine of latitude. (bottom) Scaled diameter bias as a function of latitude, calculated as the median F_D from equation 1 (solid) or equation 2 (dashed) relative to its value at the equator. The drop off in apparent bias at high latitude is because the high biases exceed the threshold in each method, and the remaining craters have lower bias.

and Hogan (2021) (the **irH1k** catalog) that found craters down to 1km, the Benedix et al. (2020) catalog has lower performance in all metrics.

I also identified a possible scaling error in the Benedix et al. (2020) catalog related either to image projection or using the incorrect pixel-to-kilometer scaling constant. I proposed a correction that rescaled to crater sizes by the correct scaling coefficient and generated the **B_Rescaled** catalog. This rescaled catalog improved in all metrics over the original catalog.

Since the validation of crater catalogs becomes increasingly difficult with their increasing size, the ground-truth comparison methods must be clearly defined and repeatable without ambiguity. In Lee (2019), I attempted to provide enough information to reconstruct the catalogs and provided detailed metric calculations and source code (Lee, 2018a). This catalog also included the matching craters from Robbins and Hynek (2012). Lee and Hogan (2021) also provided software and catalogs necessary to repeat the analysis Lee and Hogan (2021). Still, we did not identify the matching ground-truth craters or the ‘true positives’ from CDA catalogs. Similarly, Benedix et al. (2020) provided an accessible catalog of craters but with no software or identifications of ground-truth craters, and a more narrative description of the comparison methods.

Since these CDAs are now used to study craters smaller than existing catalog limits, there are no ground-truth catalogs. It has become necessary to use independent neural networks or other tools to provide supporting validation of new catalogs. In Lee and Hogan (2021), we used multiple networks trained on different input datasets to increase the overall performance. In Lee (2018b), I used multiple networks on the same high-resolution DTM dataset to achieve the same result. In Lagain, Bouley, et al. (2021), new web-based tools were developed to validate an existing catalog and found several thousand new craters and possible mis-identifications. These additional validation tools from secondary networks or manual validation efforts should be considered necessary in future studies to provide confidence in new crater catalogs.

Finally, since algorithm errors can arise, the source code and detailed methodology for the entire CDA should be an essential part of future research contributions. The source code and processed catalogs used in the analysis here are provided at Lee (2023b).

Open Research Section

The two published crater catalogs compared here can be found at Benedix et al. (2020) and Lee and Hogan (2021) and links therein. Software and catalog comparison data for this work is available at <https://doi.org/10.5683/SP3/AUJMHR>.

Acknowledgments

The author thanks Benedix et al. (2020) and Robbins and Hynek (2012) for releasing their crater catalogs in easily accessible formats. The Natural Sciences and Engineering Research Council of Canada funded part of this project. The author thanks S. J. Robbins and an anonymous reviewer for valuable comments that help clarify the article.

References

- Benedix, G. K., Lagain, A., Chai, K., Meka, S., Anderson, S., Norman, C., . . . Tan, T. (2020, March). Deriving Surface Ages on Mars Using Automated Crater Counting. *Earth and Space Science*, 7(3). doi: 10.1029/2019EA001005
- Diakogiannis, F. I., Waldner, F., Caccetta, P., & Wu, C. (2019). ResUNet-a: A deep learning framework for semantic segmentation of remotely sensed data. *Arxiv*.
- Fairweather, J. H., Lagain, A., Servis, K., Benedix, G. K., Kumar, S. S., &

- Bland, P. A. (2022, July). Automatic Mapping of Small Lunar Impact Craters Using LRO-NAC Images. *Earth and Space Science*, 9(7). doi: 10.1029/2021EA002177
- Giannakis, I., Bhardwaj, A., Sam, L., & Leontidis, G. (2023, April). *Deep learning universal crater detection using Segment Anything Model (SAM)* (No. arXiv:2304.07764). arXiv. doi: 10.48550/arXiv.2304.07764
- Goodfellow, I., Bengio, Y., & Courville, A. (2016). *Deep Learning*. MIT Press.
- Lagain, A., Benedix, G. K., Servis, K., Baratoux, D., Doucet, L. S., Rajšić, A., . . . Miljković, K. (2021, November). The Tharsis mantle source of depleted shergottites revealed by 90 million impact craters. *Nature Communications*, 12(1), 6352. doi: 10.1038/s41467-021-26648-3
- Lagain, A., Bouley, S., Baratoux, D., Marmo, C., Costard, F., Delaa, O., . . . Gamblin, O. (2021, August). Mars Crater Database: A participative project for the classification of the morphological characteristics of large Martian craters. In W. U. Reimold & C. Koeberl (Eds.), *Large Meteorite Impacts and Planetary Evolution VI* (Vol. 550, p. 0). Geological Society of America. doi: 10.1130/2021.2550(29)
- Latorre, F., Spiller, D., Sasidharan, S. T., Basheer, S., & Curti, F. (2023, April). Transfer learning for real-time crater detection on asteroids using a Fully Convolutional Neural Network. *Icarus*, 394, 115434. doi: 10.1016/j.icarus.2023.115434
- Lee, C. (2018a). *Crater Catalogs and software for "Automated crater detection on Mars using deep learning"*.
- Lee, C. (2018b). Martian Crater Identification Using Deep Learning. In *American Geophysical Union Fall Meeting* (p. P41D-3768).
- Lee, C. (2019). Automated crater detection on Mars using Deep Learning. *Planetary and Space Science*. doi: 10.1016/j.pss.2019.03.008
- Lee, C. (2023a). *Replication Data for: Comparison of automated crater catalogs for Mars from Benedix et al. (2020) and Lee and Hogan (2021)*. borealisdata.ca: Dataverse. doi: 10.5683/SP3/AUJMHR
- Lee, C. (2023b, July). *Replication Data for: Comparison of automated crater catalogs for Mars from Benedix et al. (2020) and Lee and Hogan (2021)*. Borealis. doi: 10.5683/SP3/AUJMHR
- Lee, C., & Hogan, J. (2020). *Crater Catalogs and software for "Automated crater detection with human level performance"*. doi: 10.5683/SP2/CFUNII
- Lee, C., & Hogan, J. (2021, February). Automated crater detection with human level performance. *Computers and Geosciences*, 147, 104645. doi: 10.1016/j.cageo.2020.104645
- Malin, M. C., Bell III, J. F., Cantor, B. A., Caplinger, M. A., Calvin, W. M., Clancy, R. T., . . . Wolff, M. J. (2007). Context Camera Investigation on board the Mars Reconnaissance Orbiter. *Journal of Geophysical Research: Planets*, 112(E5). doi: 10.1029/2006JE002808
- Redmon, J., Divvala, S., Girshick, R., & Farhadi, A. (2016, June). You Only Look Once: Unified, Real-Time Object Detection. In *2016 IEEE Conference on Computer Vision and Pattern Recognition (CVPR)* (pp. 779–788). doi: 10.1109/CVPR.2016.91
- Redmon, J., & Farhadi, A. (2018, April). *YOLOv3: An Incremental Improvement* (No. arXiv:1804.02767). arXiv. doi: 10.48550/arXiv.1804.02767
- Robbins, S. J. (2017). Progress on old and new: D > 1km crater catalogs for Mars and Moon. In *Planetary Crater Consortium 8* (pp. 1–2). doi: 10.1111/maps.12895.
- Robbins, S. J., & Hynek, B. M. (2012). A new global database of Mars impact craters larger than 1 km: 2. Global crater properties and regional variations of the simple-to-complex transition diameter. *Journal of Geophysical Research E: Planets*, 117(6), 1–21. doi: 10.1029/2011JE003967

- Salamunićcar, G., Lončarić, S., & Mazarico, E. (2012). LU60645GT and MA132843GT catalogues of Lunar and Martian impact craters developed using a Crater Shape-based interpolation crater detection algorithm for topography data. *Planetary and Space Science*, *60*(1), 236–247. doi: 10.1016/j.pss.2011.09.003
- Silburt, A., Ali-Dib, M., Zhu, C., Jackson, A., Valencia, D., Kissin, Y., . . . Menou, K. (2019). Lunar crater identification via deep learning. *Icarus*, *317*, 27–38. doi: 10.1016/j.icarus.2018.06.022
- Yang, S., & Cai, Z. (2022). High-Resolution Feature Pyramid Network for Automatic Crater Detection on Mars. *IEEE Transactions on Geoscience and Remote Sensing*, *60*, 1–12. doi: 10.1109/TGRS.2021.3104925